13th ewtec 2019 Proceedings of the 13th European Wave and Tidal Energy Conference 1-6 Sept 2019, Naples, Italy

Improving tidal turbine efficiency using winglets

Anna M. Young, Amanda S. M. Smyth, Viraj Bajpai, Ruth F. Augarde,
Judith R. Farman, and Carl L. Sequeira

***Abstract*—The cost effectiveness of a tidal stream turbine can be improved by maximising the power extracted for a given rotor diameter. This paper presents a numerical and experimental study showing that winglets could be used to this end. The numerical simulations were conducted using Tornado, a vortex lattice code, which can model the interaction between different spanwise sections unlike Blade Element Momentum methods. Tornado was used to identify the important winglet design parameters such as dihedral angle. Three metrics were used to evaluate the designs: power coefficient, hydrodynamic efficiency and structural efficiency, thus assessing their effectiveness not only in relation to power extraction but also to the blade material cost per kilowatt. It was found that the three metrics give different optimum winglet designs. Tornado cannot capture viscous effects and so an experimental study was conducted on four designs. These were tested on a small-scale horizontal axis turbine in the Ifremer flume tank. In all tests, the pressure side winglets offered an improvement in performance over the datum case, though the hydrodynamic failure was more abrupt at low tip-speed ratios. The suction surface winglets were inferior to the datum design. The impact of winglets on the blade spanwise flow was found to have a significant effect on the amount of loss generated due to secondary kinetic energy in the wake. The importance of spanwise flow in determining turbine performance highlights the need for fully 3D blade design codes. The inviscid code used in this paper could complement existing quasi-3D design tools.**

***Index Terms*—Blade hydrodynamics, structural loading, turbine design.**

I. Introduction

TIDAL turbines typically operate in constrained channels where their diameter is restricted by the water depth. This means that it is important to extract as much power as possible from a given rotor swept area.

Winglets are routinely used on aircraft to increase the lift generated by a wing of constrained span, and they may offer a similar benefit on tidal turbine blades. Alternatively, winglets may allow the rotor diameter to be decreased without sacrificing power output. Winglets may also improve the efficiency of a turbine if they can be designed to reduce circumferential non-uniformity in the blade tip region, and therefore reduce the total rotor wake mixing loss [1].

At the end of any wing with finite span, there is a rapid drop in lift, or circulation, and so a tip vortex will form [2]. This vortex generates induced drag and thus reduces the efficiency of the wing. Winglets reduce the induced drag by altering the spanwise flow along the finite wing length to decrease the rate of change of circulation along the wing and hence decrease the total lost energy due to vorticity trailed into the wake [3], [4]. The disadvantages of winglets are that there is a penalty in terms of parasitic drag due to the increased wetted area and that the structural load on the wing increases.

Historically, end-plates have been used to reduce the tip vortex by acting as a fence to separate the suction and pressure surfaces of the wing, thereby minimising spanwise flow. In contrast, a winglet is designed to produce a 'flowfield that actively interacts with that of the main wing to reduce the amount of spanwise flow' [5]. Importantly, this interaction means that the impact of a winglet can vary considerably with operating condition.

The change in tip flowfield manifests itself as a junction vortex, which is usually much smaller in size and magnitude than the tip vortex, and a modified tip vortex that is displaced with respect to the wing's lifting surface [3]. This can enhance the lifting capability of the outer wing span, which, for a turbine, increases power extraction.

By altering the flowfield, winglets can reduce spanwise flow effects while having a far smaller wetted area than an equivalent end-plate, thereby minimising the increase in parasitic drag [5]. This flowfield modification therefore also allows a winglet to reduce the induced drag more effectively than a "simple wingtip extension with the same structural penalty" [2]. The trade-off between aerodynamic performance and structural loading is the main design metric of an aircraft winglet, and an equivalent structural efficiency for a tidal turbine is described in Section IV-A.

While winglets have been used in the aerospace industry for many years (see for example [2], [5]), and have recently been employed on wind turbines [6], the winglet design process is imprecise and is based primarily on empirical rules or trial-and-error. This is partly because winglet performance is highly sensitive to turbine operating conditions [4].

In this paper, it is shown that winglets can be used to enhance the performance of a tidal turbine. First, an inviscid design code is used to investigate the winglet

Paper ID: 1635; Track: Tidal Device Design. The research leading to these results has received funding from the EPSRC and from the European Union Horizon 2020 Framework Programme (H2020) under grant agreement no 731084.

A. Young was at the University of Cambridge, Whittle Laboratory, Cambridge, CB3 0DS, UK. She is now at the University of Bath (e-mail: amy32@bath.ac.uk).

A. Smyth (asmms2@cam.ac.uk) and J.Farman (jrf55@cam.ac.uk) are at the Whittle Laboratory.

V. Bajpai (vb343@cantab.net), R. Augarde (rfa27@cantab.net) and C. Sequeira (cls65@cantab.net) were at the Whittle Laboratory.

design space, with particular emphasis on the dihedral angle. From the results of the parametric study, four different winglets are selected for experimental testing on a model tidal turbine. The performance change is measured across the speed range of the turbine. Rotor phase-locked PIV is then used to examine the changes in the radial and axial flow non-uniformity and to explain the observed performance changes.

II. Nomenclature

Symbol	Quantity	Unit
$\dot{m}$	mass flow	kgs^{-1}
p	static pressure	Pa
p_{in}	inlet pressure	Pa
r	radius	m
u'	perturbed velocity component	ms^{-1}
A	turbine swept area	m^2
C	material cost per unit volume	$\$\mathrm{m}^{-3}$
C_{P}	power coefficient	-
C_{T}	thrust coefficient	-
$\dot{E}$	secondary kinetic energy deposition rate	W
$\dot{E}_{\text{vortex}}$	transverse SKE deposition rate	W
$\dot{E}_{\text{pressure}}$	pressure defect work rate	W
F_x	axial force	N
L	blade length	m
M	root bending moment	Nm
Q	torque	Nm
T	thrust	N
TSR	tip-speed ratio $= \frac{\omega R_{\text{tip}}}{U_\infty}$	-
U	local velocity	ms^{-1}
U_∞	free-stream velocity	ms^{-1}
η_{hydro}	hydrodynamic efficiency	-
η_{struct}	structural efficiency	-
ρ	density of water	kgm^{-3}
σ	yield stress	MPa
ω	rotational velocity	rads^{-1}
x, r, θ	coordinate directions: used as subscripts	

III. Winglet design code - Tornado

In order to investigate the effect of winglets on the performance and efficiency of a tidal turbine, a parametric study was conducted using Tornado: a 3D vortex lattice code developed by Melin [7] for aircraft wing designs. The code divides the blade into a lattice of panels, each with an associated horseshoe vortex and prescribes the motion of the trailing vortices shed from the blade into the wake. By dividing the blade up in this way, the conservation equations can be turned into a matrix equation ($\mathbf{A\Gamma} = \mathbf{b}$, where $\mathbf{A}$ is the matrix for the influence of all vortex lines on all panels in the flow, $\mathbf{\Gamma}$ is the matrix of circulations of each panel, and $\mathbf{b}$ is the flow velocity vector at each panel). Unlike the quasi-3D Blade Element Momentum methods typically used for tidal turbine design, vortex lattice methods model the interaction between different spanwise sections of the blade and so give information on the effect of a tip section change on the whole blade performance.

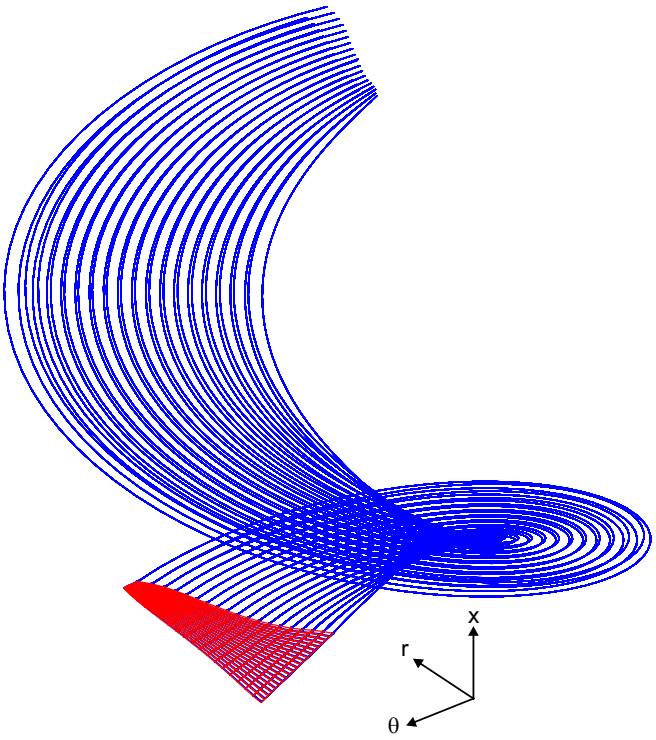

Fig. 1. Diagram showing the blade and wake as simulated by Tornado. Vortex lines are shown in blue, the blade is shown in red.

The advantage of Tornado over a viscous solver is its speed - designs can be evaluated in under a minute on a laptop computer. There are, however, various assumptions made about the flow. Most importantly, the code is inviscid and so the flow remains fully attached at all times.

Figure 1 shows the blade used for this study. The vortex panels on the blade are shown in red, while the paths of the wake vortices are shown in blue (individual collocation points are omitted for clarity). Tornado was designed for aircraft wings at low angles of attack and with limited rotation, and so the wake vortex lines were straight and followed the freestream flow direction. The modelling of a tidal turbine therefore required modification to the code for the motion of the wake. It can be seen in Fig. 1 that the wake is helical and comes off the trailing edge smoothly in the relative flow direction.

The blade section loading distributions obtained from Tornado were validated by comparing simulations with very large radius (Where 3D effects are minimal) against outputs from the 2D coupled Euler-Boundary Layer solver, MSES. For further details, see [8].

IV. Parametric study using Tornado

The datum design tested with Tornado was the model tidal turbine described in Section V, and the winglet sections were generated by extending the blade with identical section shape and a linear extrapolation of the tip-region chord and thickness distributions. The additional blade section was then rotated to different dihedral angles to create a winglet, with a bend radius of 1 cm (3% of the original blade span). A diagram

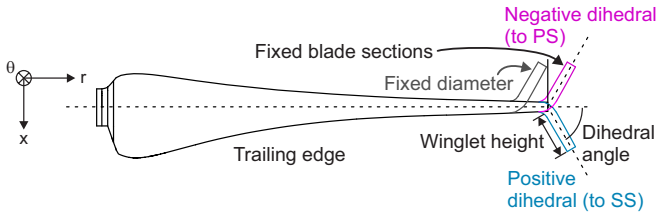

Fig. 2. Diagram of the definition of dihedral angle used in this paper.

of the turbine blade is shown in Fig. 2, where the definition of dihedral angle and the sign convention are both shown. Note that positive dihedral is towards the suction surface (i.e. the conventional direction for aircraft winglets). Also shown on Fig. 2 is the definition of winglet height. Two winglet heights were considered - 10% and 20% of the original blade span - with dihedral angles from -90° to +90°.

For the parametric study, the radius at which the winglet began was held constant and the total diameter of the turbine was allowed to vary. This is shown in Fig. 2 by the blue 'fixed sections' tip as opposed to the grey 'fixed diameter' tip. This means that a winglet with 0° dihedral represents a radial extension of the blade. This change in diameter was accounted for when non-dimensionalising by turbine swept area in the results presented below.

A. Performance parameters

Aircraft designers typically trade off the reduction in induced drag due to a winglet with the increase in structural load. For a tidal turbine, the trade-off is less straightforward as the blade is highly twisted and the important parameters are the torque, blade root bending moment and thrust.

In this work, three performance parameters have been considered. First, the power coefficient, C_P:

$$C_\mathrm{P} = \frac{Q\omega}{\frac{1}{2}\rho U_\infty^3 A} \tag{1}$$

where Q is the rotor torque, ω the rotational speed, U_∞ the flow velocity and A the rotor swept area. C_P is a useful measure of the power generated as a fraction of the energy flowing through the turbine swept area, and therefore of how efficient the rotor is at making use of the power available. It does not, however, give any indication of the loading incurred by the turbine in generating the power, or of the amount of power removed from the flow.

The second efficiency measure is the hydrodynamic efficiency, η_hydro, which is a measure of the ratio of the power coefficient to the thrust coefficient, C_T:

$$C_\mathrm{T} = \frac{T}{\frac{1}{2}\rho U_\infty^2 A} \tag{2}$$

where T is the thrust on the turbine. The power removed from the flow is taken to be TU_∞, such that:

$$\eta_\mathrm{hydro} = \frac{Q\omega}{TU_\infty} = \frac{C_\mathrm{P}}{C_\mathrm{T}} \tag{3}$$

The power lost from the flow, TU_∞, is equal to the power generated, $Q\omega$, plus any loss generated in the flow by the turbine. This means that the hydrodynamic efficiency tells a designer how much loss is generated and therefore the thrust that the turbine has to withstand in order to generate a given amount of power.

The issue with the hydrodynamic efficiency is that it

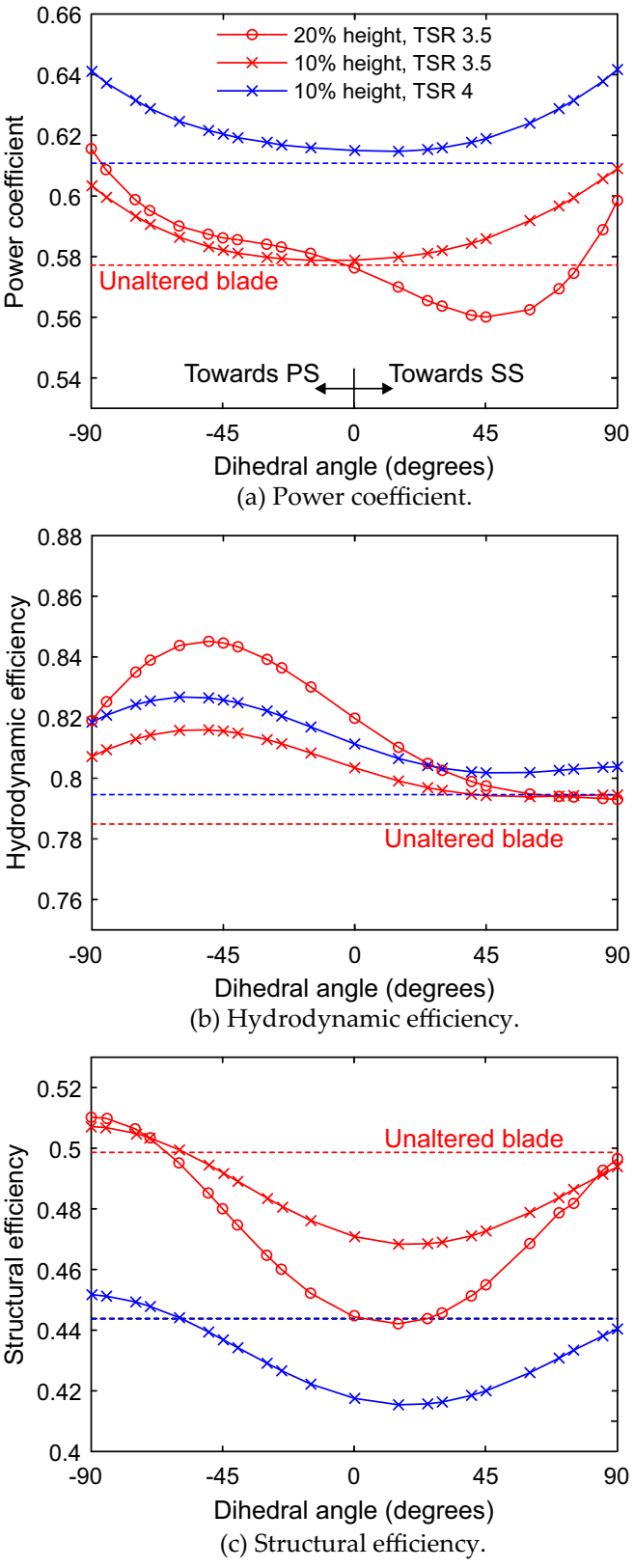

(a) Power coefficient.

(b) Hydrodynamic efficiency.

(c) Structural efficiency.

Fig. 3. Results from Tornado simulations showing the effect of winglet dihedral angle on turbine performance. It can be seen that the trade-off between power coefficient and structural efficiency changes with dihedral angle.

compares a moment (torque) with a force (thrust) and therefore encourages the extraction of more power at a higher radius. This gives a more hydrodynamically efficient turbine, but at the cost of increased root bending moment. To account for this, a third efficiency measure is used; the structural efficiency, η_{struct}:

$$\eta_{\text{struct}} = \frac{Q}{M} \tag{4}$$

where M is the blade root bending moment. This measure of efficiency gives a fairer comparison between torque (and therefore power, for a given rotational speed) and root bending moment (and therefore structural loading).

Figure 3 shows the effect of winglet dihedral angle, height and tip-speed ratio (TSR) on the three performance parameters derived above. In every case, the datum blade performance is shown as a dotted line (blue for TSR 3.5 and red for TSR 4).

Considering first the power coefficient (Fig 3(a)), it can be seen that, for the 10% span winglets (crosses), the power coefficient always increases when a winglet is applied. The largest increases in power coefficient are at the extremes ($\pm 90^\circ$ dihedral). This shows that the increased power generated at the tips is almost cancelled out by the increase in rotor swept area for moderate dihedral angles, but that the high dihedral angle designs make more efficient use of the space and therefore the power coefficient increases.

The effect of TSR on the trends is minimal, with the power generated at TSR 4 (blue line) having the same shape as the result for TSR 3.5 (red line), but shifted up due to the higher power output of the datum blade at this operating point.

With a longer winglet (20% span, red line with circles), the trend is now asymmetric, and the power coefficient is reduced relative to the datum for designs with positive dihedral angles between 0° and 70°. This again shows the importance of efficient use of space, as the swept area increases faster than the power output for the longer winglets with moderate positive dihedral.

Turning now to the hydrodynamic efficiency (Fig 3(b)), it can be seen that Tornado predicts all the winglet designs to give an improvement against the datum design. This means that the increase in power produced outweighs any increase in hydrodynamic loss. The peak hydrodynamic efficiency is at a dihedral angle of -50°. The asymmetry in the hydrodynamic efficiency with dihedral angle suggests that, while the shorter (10% length) suction surface winglets are generating approximately the same amount of additional power as the pressure surface winglets, there is an asymmetry in the amount of loss generated. The differences in loss may be due to the effect of the different winglets on the spanwise flow and will be discussed in Section V-C.

As with the power coefficient, the effect of TSR is simply to shift the hydrodynamic efficiency curve by shifting the datum point. The effect of winglet height on hydrodynamic efficiency is more pronounced for negative dihedral angles than it is for positive angles.

Finally, the structural efficiency is shown in Fig 3(c)). Unlike the first two efficiency measures, the effect of winglets is generally to reduce the structural efficiency. This is because more work is being done at a higher radius, which increases the torque but also has a corresponding effect on the blade root bending moment. Again, the trend is asymmetric, with negative dihedral winglets offering higher efficiency than positive dihedral designs. The only winglets to offer improved structural efficiency over the datum design are those with a negative dihedral angle of at least 60°, while the designs with positive dihedral of 90° almost achieve parity with the datum case.

While the effect of TSR on the trend in structural efficiency with dihedral angle is minimal, it is interesting to note that the datum blade has inferior structural efficiency with higher TSR (this is opposite to the effect of TSR on power coefficient and hydrodynamic efficiency).

Comparing the three trends, it can be seen that power coefficient and hydrodynamic efficiency can be increased by using winglets, but that this increase is often at the expense of structural efficiency. The trade-off between structural efficiency and power coefficient can be quantified via the blade material cost, as will be discussed in the next section.

B. Cost trade-off

Using the metrics from the previous section, an increase in power coefficient can be traded off against reduced structural efficiency in order to balance material cost with power generated. The trade-off is, however, not linear and will depend on the precise structural design of the turbine blades. In this section, we estimate a relationship between cost, structural efficiency and power coefficient by assuming that the blade is supported by a cylindrical spar at the root and that material costs for the whole blade scale with the amount of material used in this spar. This is likely to be a conservative estimate, as the blade root is the most adversely affected by increased loading.

Considering a spar of radius r and yield stress σ, the maximum bending moment that can be sustained is:

$$M = \frac{\sigma \pi r^3}{4} \tag{5}$$

taking the material cost of the spar to scale with size, the material cost per kilowatt (kW) is:

$$\text{Cost per kW} = \frac{C \pi r^2 L}{Q \omega} \tag{6}$$

where C is the material cost per unit volume and L is the blade length. Eliminating the free variable, r, from Equation 6 using Equation 5 and grouping constants gives:

$$\text{Cost per kW} = \frac{M^{2/3}}{Q} \frac{C \pi L}{\omega} \left[\frac{4}{\sigma \pi}\right]^{2/3} \tag{7}$$

substituting for C_P and η_{struct} and eliminating constants (assuming constant flow speed and TSR) gives:

$$\text{Cost per kW} \propto \left(\frac{1}{\eta_{struct}}\right)^{2/3} \left(\frac{1}{C_P}\right)^{1/3} \quad (8)$$

i.e. in order to minimise the cost per kW, $(\eta_{struct})^{2/3}(C_P)^{1/3}$ must be maximised. A more sophisticated model could be used to account for the actual geometry of a turbine blade, but the principle remains the same - the trade off between material cost and power generation can be captured via the method above.

Fig. 4 shows structural efficiency against power coefficient for winglets at different angles (red lines) and blade extensions (blue lines). A line of constant material cost per kW generated is plotted as a dashed line passing through the datum design point. According to the model, any design above the dashed line offers superior material cost per unit power generated. For the 20% span designs (Fig. 4(a)), this means the 90° suction surface winglets and the pressure surface winglets from approximately 60° to 90°. Blade extensions, on the other hand, offer inferior cost per unit power because they increase the spanwise position at which bending moment is generated without offering a substantial increase in torque at the outer sections.

The trend is similar with shorter winglets, as shown in Fig. 4(b), though slightly more of the designs are predicted to give improved material cost per kW over the datum. The effect of TSR is also shown in Fig. 4(b); it can be seen that the same designs outperform the datum blade, but the curves are shifted down and to the right, reflecting the decrease in structural efficiency and increase in power coefficient with TSR. In all cases, the winglet curve intersects the blade extension curve at 0° dihedral, because a zero-degree winglet is equivalent to a blade extension.

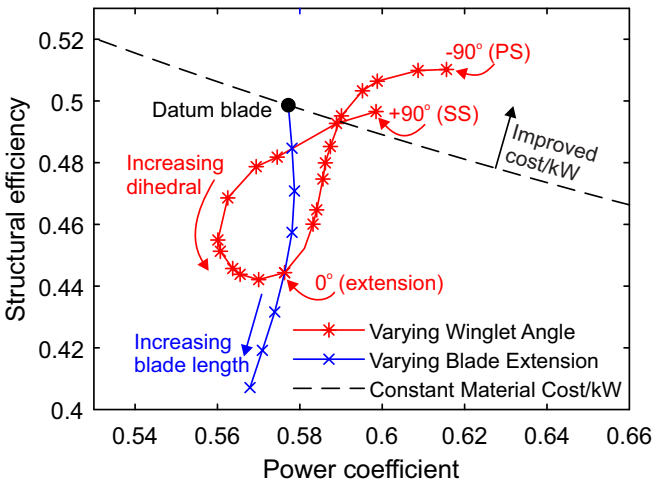

(a) Winglet height 20% span, TSR 3.5.

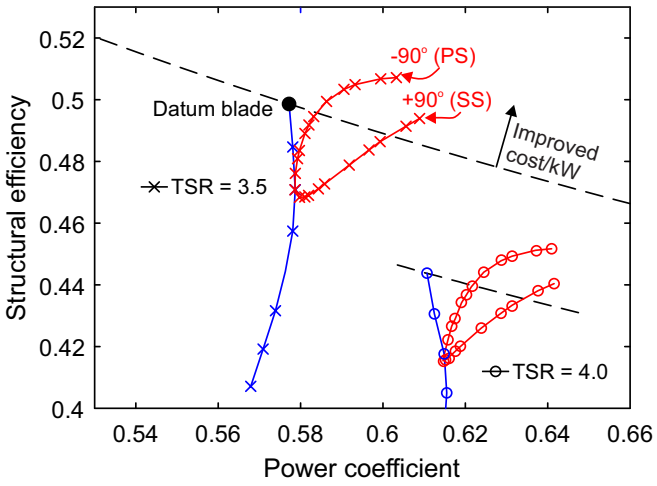

(b) Winglet height 10% span, TSR 3.5 and 4.0.

Fig. 4. Graph of structural efficiency against power coefficient for winglets and blade extensions. It can be seen that some winglet angles offer an improved balance of structural efficiency and power over the datum blade.

V. Model Turbine Tests

In order to understand the impact of viscous effects on the results discussed above, four different winglet designs were tested on a small-scale, three bladed horizontal axis turbine. The turbine has a rotor tip diameter of 700 mm and a hub diameter of 88 mm. The rotor shaft is connected to a generator and power inverter via a gearbox. With this drivetrain, the maximum turbine speed is 230 rpm. The blades are representative of a typical tidal turbine, and with the datum blade design, peak power is produced at a TSR of 4.

The winglet designs tested are shown in Fig. 5, along with the mounting arrangement (Fig. 5(a)). It can be seen that the outer 30% of the blade span is interchangeable and that the different designs are held in place by a threaded bar accessed from the turbine hub. The position of the tip portion is fixed by two locating pins. A rubber gasket seals the gap between the main blade and the tip.

Four designs were selected for testing: 90° to the suction surface, 90° to the pressure surface and two designs at 60° to the pressure surface (one with the same outer diameter as the other designs and one with the same blade sections). In all cases the winglet height was 10% of the blade length. These designs were selected because they span the entire range of dihedral angles and because they were all predicted by Tornado to give improved performance over the datum design (see Fig. 4).

The turbine was tested in the flume tank at Ifremer, Boulogne-sur-Mer, France. The working section is 4 m wide, 2 m deep and 8 m long. The turbine was mounted at mid-depth and away from the tank endwalls. The flow speed was set to 1 m/s, and the turbulence intensity was 3%. At a TSR of 4, this gave a mid-span Reynolds number of 175,000 (based on chord).

The turbine drivetrain is equipped with a torque transducer which measures the torque on the blades, and the turbine was mounted on a 6-axis load cell to measure the thrust. These are shown in red on Fig. 6.

As well as torque and thrust measurements, the evolution of the wake was measured using PIV for all of the designs, apart from the 60° fixed section winglets, (which were not tested due to time constraints). A GEMINI-LIKE Nd-YAG Laser was used with power

of 200 mJ per probe and wavelength of 532 nm. The laser was synchronized with a camera (FLOW SENS EO-2M) with a resolution of 1600pix × 1200pix and a time-step between images of 1600 μs.

The PIV set up is shown in Fig. 6. The laser produced an axial-vertical (x-z) plane of light aligned with the rotor hub in the transverse direction and and the camera captured an area covering approximately 950 mm x 725 mm (1.4 x 1.0 rotor diameters) from the hub to below the tip of the blade. The spatial resolution of the measurements was approximately 10 mm in each direction. The field of view extended over the rotor plane in the axial direction and so the turbine was painted black to minimise reflections. Despite this, the noise content was high in the data from within 0.1 diameters of the rotor.

The PIV system was used to obtain rotor phase-locked wake profiles. This was achieved by using a once-per-revolution square wave pulse on the rotor shaft to trigger the PIV system. By using a variable time delay, phase-locked data were acquired every 3° over a complete rotor blade passing (120°). For each rotor phase, 200 images were acquired to enable an average to be taken such that the tip vortex and other periodic flow features could be visualised at different axial planes, and the rotor wake loss calculated.

The data were post processed in Dantec Dynamic Studio using a cross-correlation method. Unfortunately, an issue with the Dantec trigger module meant that a substantial proportion of the data had to be discarded via a semi-automated process. The data shown here has typically been produced from 50-150 repeats at each phase, which is sufficient to eliminate noise and stochastic features and to show the periodic flow features clearly.

A. Performance curves

The performance of the turbine was measured across its TSR range in terms of both power coefficient and thrust coefficient. The power coefficient obtained with each of the five tip designs is shown in Fig. 7. It can be seen that, compared with the datum blade (black line), the peak power is increased by all three pressure surface winglet designs (60° - fixed section and fixed diameter - and 90°), and that peak power output has shifted from a TSR 3.5 to 4 in the case for all three designs. The suction surface winglet, however, gives a lower peak power than the datum.

At TSR 3, the pressure surface designs generate less power than both the datum case and the suction surface winglets. This earlier drop off in power suggests that the increased loading due to the pressure surface winglets is leading to large-scale separation at a lower incidence than it would otherwise occur.

Turning now to the thrust measurements, Fig. 8 shows that, unlike the case of the torque measurements, the trend is consistent across the TSR range, and the difference between designs increases with TSR. The 90° suction surface design produces the most thrust, while the 60° pressure surface (fixed diameter) design produces the least, with the other two designs (60° fixed section and 90° pressure surface) lying in between the datum blade and the suction surface design. Considered in tandem with with the power coefficient measurements, this shows that the 90° suction surface winglets are tending to produce less power for more loss, while the pressure surface designs give an improved hydrodynamic efficiency.

The results for hydrodynamic efficiency (the ratio of power coefficient to thrust coefficient - equation 3) are shown in Fig. 9. As suggested by the power and thrust measurements discussed above, the peak efficiency is higher than the datum for all designs apart from the 90° suction surface winglets. This shows that the extra thrust generated by the pressure surface winglets is outweighed by the increased power in terms of the efficient use of a finite body of water. Due to the drop in power at lower tip-speed ratios, the peak efficiency is also shifted to TSR = 4 for all the pressure surface designs.

The structural efficiency cannot be computed directly because root bending moment measurements are not available, but it can be estimated from the rotor wake measurements. This will be discussed in Section V-C.

The changes in power coefficient and hydrodynamic efficiency observed in the experiments are compared with the predictions from Tornado in Fig. 10. The experimental data is shown from TSR 3.5 and 4, while the trends from Tornado are only shown for TSR 3.5 (Tornado predicted the same trends regardless of TSR - see Fig. 3). It can be seen that the agreement between Tornado and the experiments is better at TSR 3.5 than at TSR 4. Even at TSR 3.5, Tornado predicts an increase in power coefficient for the suction surface winglet whereas the experiments give a slight drop, suggesting that there are viscous effects (e.g. a corner separation at the winglet-blade junction) which are outweighing the improvement predicted by the inviscid model.

In terms of hydrodynamic efficiency, the changes observed in the experiment are under-predicted by Tornado at both very high and very low dihedral angles. These discrepancies show that viscous effects, which are not captured in Tornado, have a profound impact on the efficiency of winglet designs.

B. Phase-averaged wake measurements

As explained above, the rotor wake was measured for four of the five designs using a PIV window in the axial-vertical plane. By triggering the data acquisition off the rotor shaft, it was possible to obtain phase-locked data and thus to generate the unsteady flowfield downstream of the rotor in terms of the axial and radial velocity. All PIV measurements were undertaken at a TSR of 4.

The axial velocity distribution in the wake can be seen in Fig. 11, which shows contours of axial velocity (normalised by freestream velocity) 0.25 turbine diameters downstream of the turbine with each of four different tip designs (datum, 90° pressure surface, 90° suction surface and 60° pressure surface with fixed diameter). In each case, the low velocity wake is seen as a region of blue extending slightly beyond the rotor

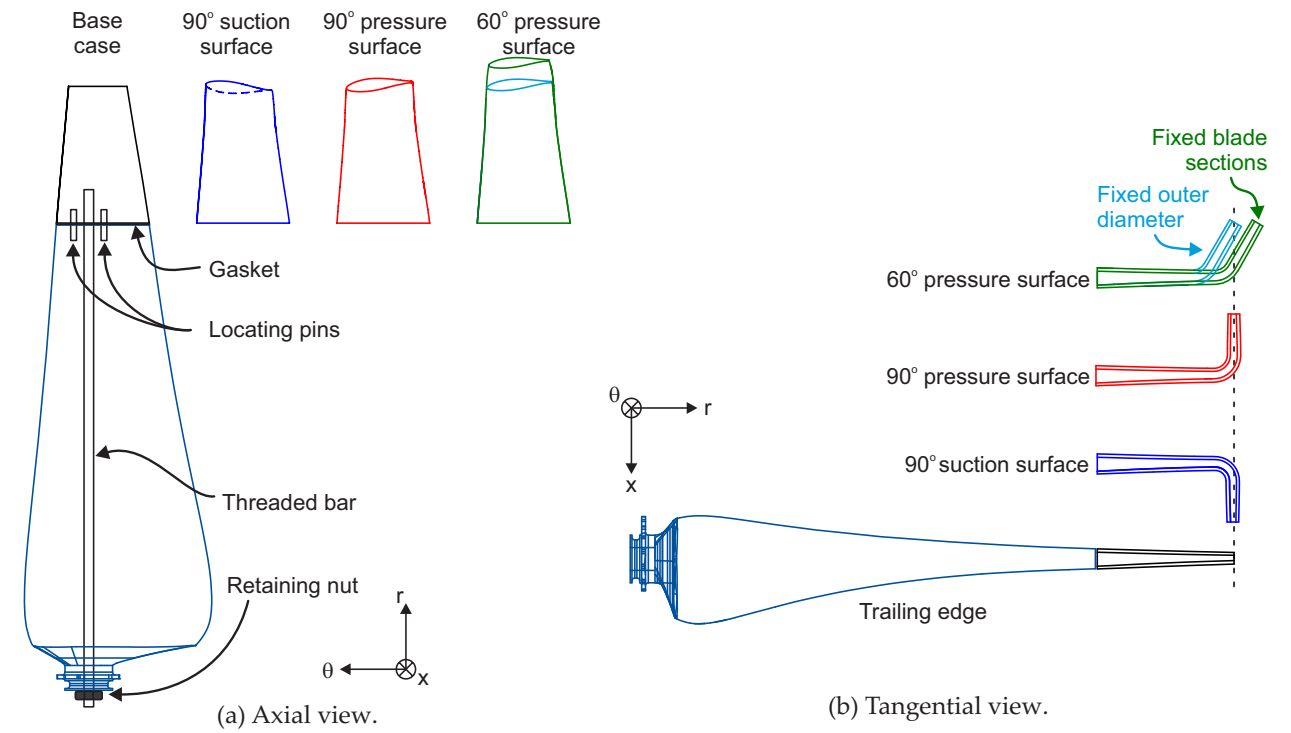

Fig. 5. Diagram of model tidal turbine blade showing the winglet designs tested and the mounting method.

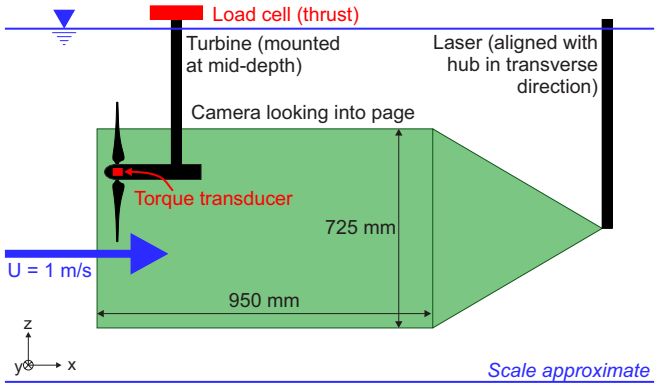

Fig. 6. Diagram of the setup for the turbine performance and PIV measurements.

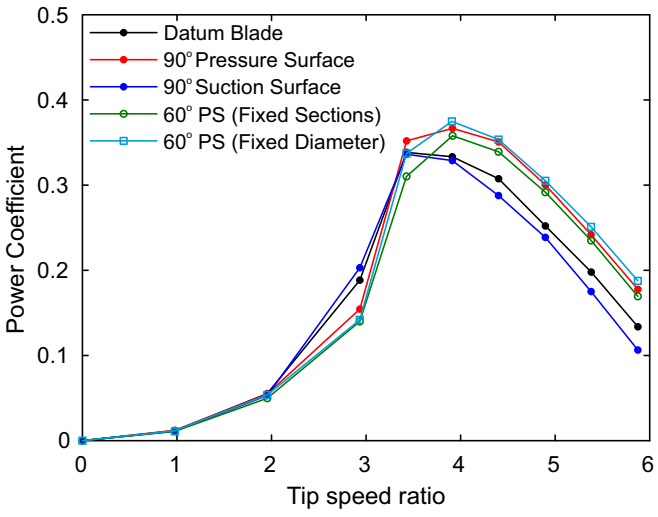

Fig. 7. Power coefficient against TSR for all five tip designs.

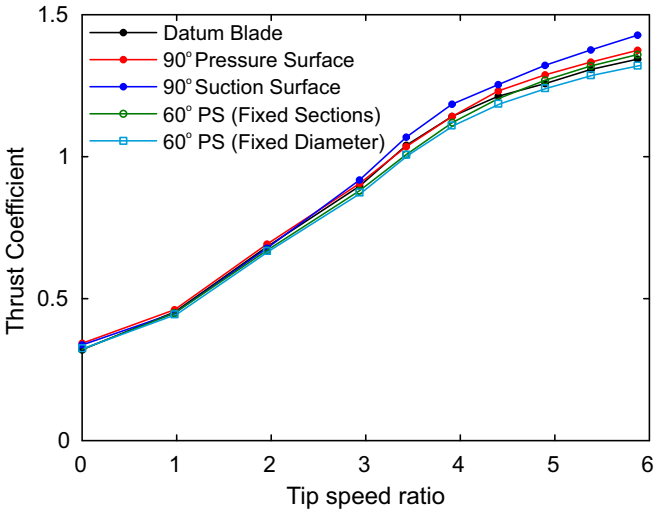

Fig. 8. Thrust coefficient against TSR for all five tip designs.

tip radius. The tip vortex can also be seen slightly further outboard, as an inner region of low velocity and an outer region of high velocity. In order to facilitate comparison between the four designs, black lines have been drawn around the contours at 30% and 120% of the freestream velocity. It can be seen that the size of the regions of high- and low-speed flow varies substantially between designs, as does their tangential position relative to the blades and to one another. This suggests that the winglets are having an impact on the formation and motion of the tip vortex, as found by Gerontakos and Lee [3].

Further evidence of the effect of winglets on the tip vortex is shown in Fig. 12, which is a set of contour plots of radial velocity 0.25 diameters downstream of the turbine. Contours of -30% of the freestream

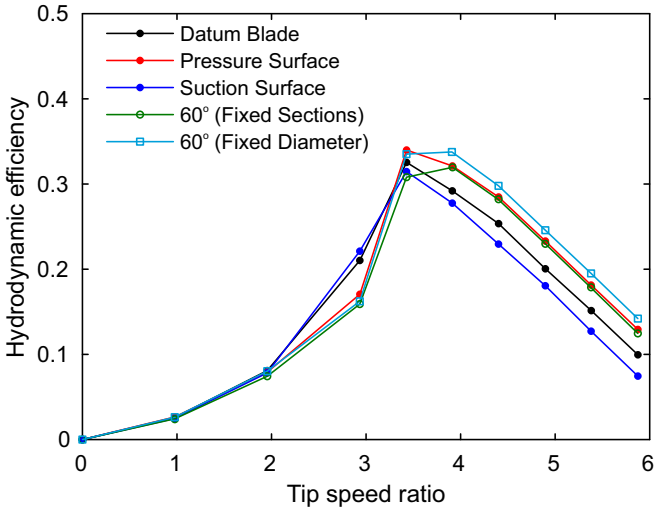

Fig. 9. Hydrodynamic efficiency against TSR for all five tip designs.

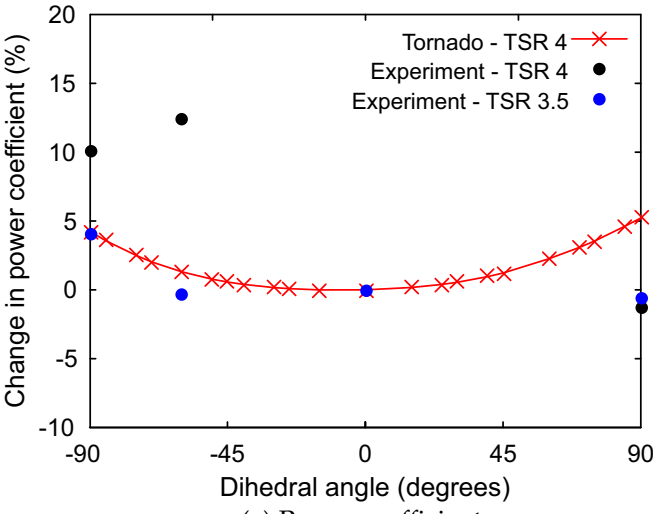

(a) Power coefficient.

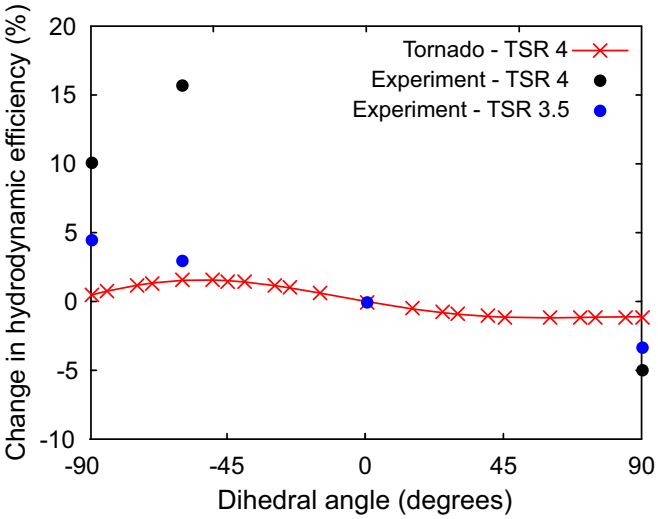

(b) Hydrodynamic efficiency.

Fig. 10. Power coefficient against tip-speed ratio for four tip designs (excludes 60° fixed diameter).

velocity are shown in black, while contours of +30% of freestream velocity are shown in white. In the datum case (Fig. 12(a)), there is a large region of positive spanwise flow just outside the rotor tip and a small region of negative flow. The winglets change the size and shape of these regions of spanwise flow, with the 60° pressure side design showing the least inward flow (smallest blue regions), and the 90° pressure side design showing the least outward flow (smallest yellow regions).

It is also worth noting that the regions of very high and very low radial velocity are at the same radius, and so the amount of flow non-uniformity would be vastly underestimated by a time-averaged measurement, which would give the circumferential mean at each radial location.

C. Loss analysis

The power extracted from the flow by a tidal turbine is equal to the useful shaft power plus the loss generated. Sequeira and Miller [9] undertook an analysis of the sources of hydrodynamic loss in a tidal turbine and found that the main source of loss was the secondary kinetic energy (SKE), i.e. the flow non-uniformity created by the turbine which must mix out downstream. The non-uniformity has components in the axial (u'_{x}), radial (u'_{r}) and tangential (u'_{θ}) directions, but is all convected at the local axial velocity, U_{x}. The mixing out of this non-uniformity creates loss, and the amount of energy lost to SKE can be calculated using a 'Trefftz' plane, as explained by Drela [10], and as undertaken by Sequeira and Miller [9]. The SKE is composed of three components - axial, vortex and pressure:

$$\dot{E} = \dot{E}_{\mathrm{axial}} + \dot{E}_{\mathrm{vortex}} + \dot{E}_{\mathrm{pressure}} \tag{9}$$

where

$$\dot{E}_{\mathrm{axial}} = \iint \frac{1}{2}\rho u'^{2}_{\mathrm{x}} U_{\mathrm{x}} dA \tag{10}$$

$$\begin{aligned}\dot{E}_{\mathrm{vortex}} &= \dot{E}_{\mathrm{radial}} + \dot{E}_{\mathrm{tangential}} \\ &= \iint \frac{1}{2}\rho \left(u'^{2}_{\mathrm{r}} + u'^{2}_{\theta}\right) U_{\mathrm{x}} dA\end{aligned} \tag{11}$$

$$\dot{E}_{\mathrm{pressure}} = \iint \left(p - p_{\mathrm{in}}\right) u'_{\mathrm{x}} dA \tag{12}$$

From the experimental data available, only $\dot{E}_{\mathrm{axial}}$ and $\dot{E}_{\mathrm{radial}}$ can be calculated, but these give valuable insight into the loss generated by the different blade designs.

The axial SKE gives a measure of the energy lost to axial non-uniformity in the flow. It can be seen from Fig. 11 that the change in velocity between the freestream and the wake is bigger than the change in velocity due to the effect of the winglets on the tip vortex. The main contribution to axial SKE is the removal of energy from the bulk flow, which is an inevitable consequence of power extraction over a finite area. This suggests that the total amount of axial SKE will be largely unaffected by the winglets. The total axial SKE is shown as the black bars in Fig. 13, which are the percentage change in axial SKE for each of the three winglet designs relative to the datum. The largest change in axial SKE is achieved by the 60° pressure surface design, but even this is only 3% of the axial SKE in the datum case.

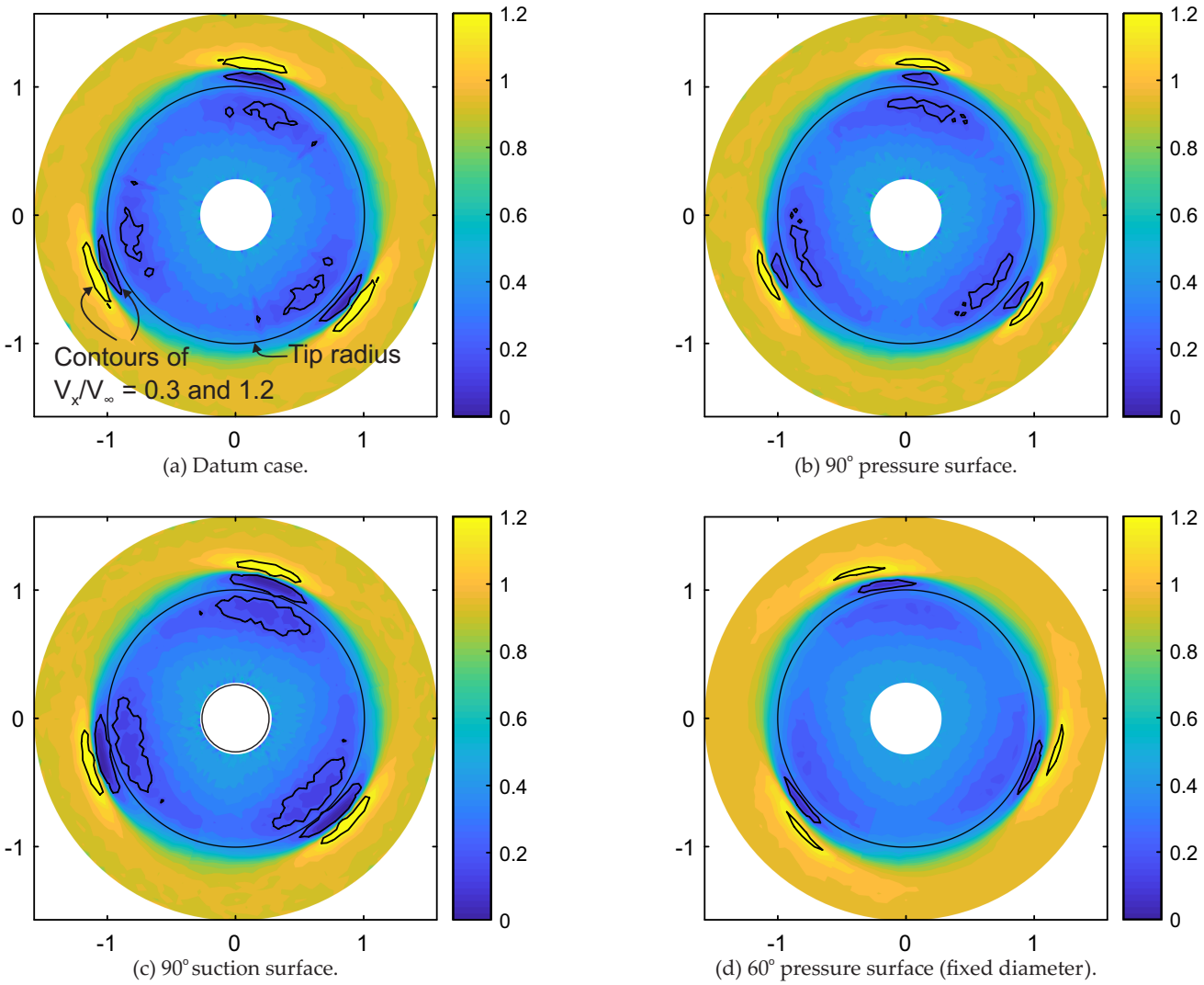

(a) Datum case.

(b) 90° pressure surface.

(c) 90° suction surface.

(d) 60° pressure surface (fixed diameter).

Fig. 11. Phase-averaged contours of axial velocity 0.25 diameters downstream of the rotor with four different tip designs.

The radial SKE is a measure of how much energy has been lost to radial (i.e. spanwise) flows, and winglets have been shown to affect the spanwise flow (see Fig. 12). An ideal turbine would generate no radial SKE, so the changes due to winglets are likely to be large relative to the datum. The percentage changes in radial SKE are shown in red in Fig. 13. It can be seen that both the 90° and 60° pressure side winglets give reductions of over 10% in radial SKE, suggesting that these winglets are acting to inhibit spanwise flow and thus reduce the amount of energy lost to radial velocity in the wake. The 90° suction surface winglet, on the other hand, gives an 8% increase in radial SKE, indicating an increase in spanwise flow and thus an increase in loss.

Another way of considering the changes in axial momentum is via the Steady Flow Momentum Equation applied to a control volume around the turbine:

$$\sum [\dot{m}U_x]_{out} - \sum [\dot{m}U_x]_{in} = \left(\sum pA\right)_x + F_x \qquad (13)$$

where $[\dot{m}U_x]_{in}$ and $[\dot{m}U_x]_{out}$ are the momentum fluxes in and out of the control volume, respectively, $(\sum pA)_x$ is the pressure acting over the axial faces of the control volume, and F_x is the axial force on the control volume (in this case, F_x will be equal and opposite to the thrust on the turbine, T). The pressure terms in this equation cannot be found from the experimental data available, but the changes in axial momentum can be found via a control volume analysis.

Any change in the axial momentum removed from the flow by the turbine will change the thrust force ($-F_x$ in equation 13). Furthermore, the radial location of the line of action of F_x will affect the bending moment generated on the blade. For each of the four designs, the force contribution from the axial momentum terms (i.e. $\int [\dot{m}U_x]_{in}\, dA$ and $\int [\dot{m}U_x]_{out}\, dA$) was calculated. The line of action of this force was then found by integrating $\int [\dot{m}U_x]_{out}\, r dA$ and assuming that the line of action of the inlet flow force must be at the same percentage of streamtube height (due to continuity). These forces and lines of action were used to estimate the contribution to the root bending moment of the axial momentum deficit. The torque generated was then non-dimensionalised by this moment, to give a form of structural efficiency.

The results of this analysis are shown in Fig. 14. Again, percentage changes relative to the datum design are shown. The black bars are from the experiments, while the red bars are the changes in structural effi-

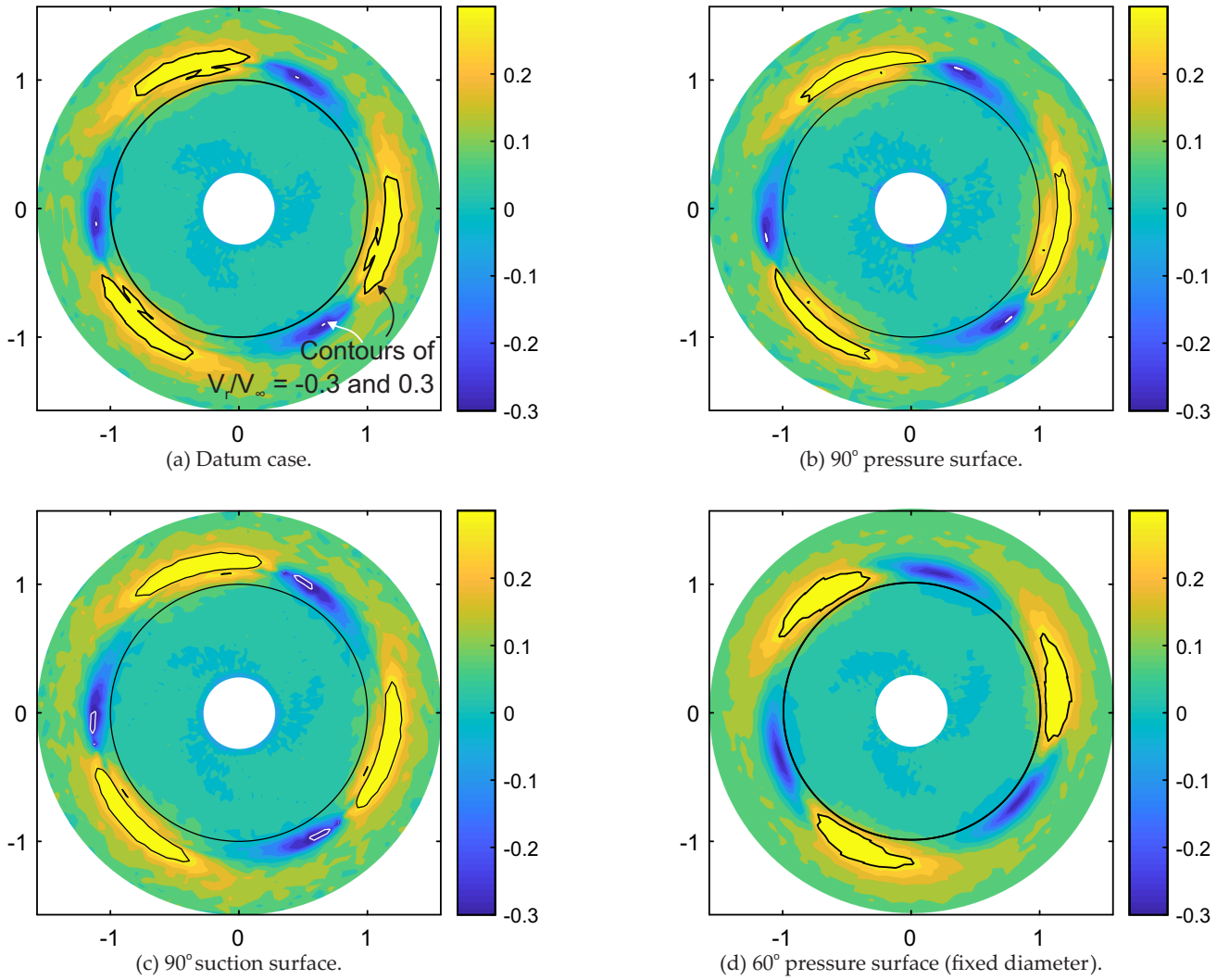

(a) Datum case. (b) 90° pressure surface. (c) 90° suction surface. (d) 60° pressure surface (fixed diameter).

Fig. 12. Phase-averaged contours of radial velocity 0.25 diameters downstream of the rotor with four different tip designs.

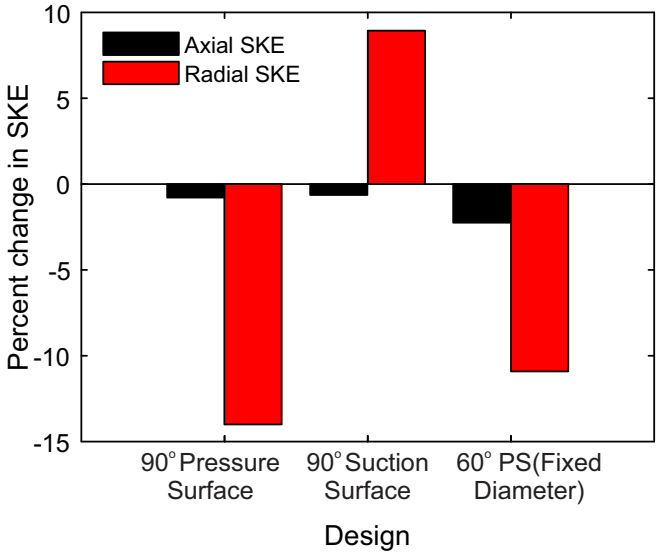

Fig. 13. Changes in axial and radial Secondary Kinetic Energy (SKE) for different designs relative to the datum.

ciency predicted by Tornado (i.e. the ratio of torque to total root bending moment). The magnitudes of the results from Tornado and the experiments would not be expected to match, because of the missing pressure terms in the experimental analysis. However, it is interesting to see that the trend is the same between the experiments and Tornado, with increased structural efficiency for the pressure surface designs and a small reduction for the suction surface design.

It is also interesting to note that the changes in bending moment due to the axial momentum deficit are substantial, despite the relatively small changes in axial SKE shown in Fig. 13. This is because, although the changes in the axial flowfield due to the winglets are small, they occur at high radius, and therefore have a significant impact on the root bending moment.

VI. Conclusions

In this paper, it has been shown that winglets can be used to increase the power generated by a tidal turbine of a given diameter, but that the dihedral angle plays a key role in determining the efficiency of a given design. In some cases, any increase in power due to the winglet is outweighed by the additional hydrodynamic loss and structural loading incurred.

An inviscid vortex panel method was used to investigate the design space and select designs for experimental testing on a small-scale tidal turbine. Three efficiency metrics were considered when assessing winglet

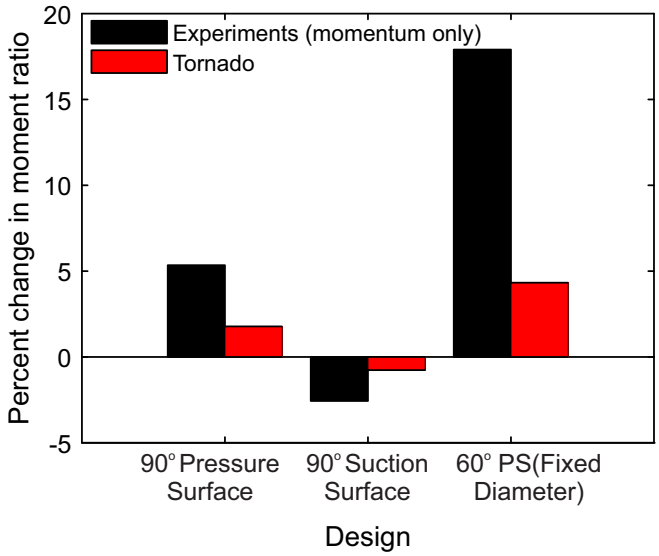

Fig. 14. Moment ratio for different designs relative to the datum.

performance. First, the power coefficient, which is the power generated as a proportion of the energy available over the rotor swept area. This first metric is important where efficient use must be made of a constrained channel. The second measure is the hydrodynamic efficiency, which is the ratio of power generated to energy removed from the flow. Hydrodynamic efficiency is important if many rows of turbines are to be deployed as increased loss will reduce the power available to downstream rows. Finally, the structural efficiency was considered. This is the ratio of torque to blade root bending moment and gives a measure of how much structural loading will be generated for a given power output.

It was found that dihedral angle has a strong influence on all three performance metrics, and that pressure surface winglets generally out-perform suction surface winglets. In almost all cases, the inviscid code predicted increased power coefficient and hydrodynamic efficiency with winglets, but the structural efficiency was generally predicted to be lower with winglets due to the increased radius at which loads were being generated. Only pressure side winglets with high dihedral angles were predicted to have higher structural efficiency than the datum case.

The trade-off between material cost and power can be estimated by considering the power coefficient and the structural efficiency together. The trade-off is not linear, but depends on the construction of the blades. In this work, a simple model was used, which predicted that winglets with high dihedral angles in either direction would give a lower cost per kilowatt of power generated.

Four different winglets were chosen for testing on a model-scale turbine, all of which were predicted by the inviscid model to give improved performance relative to the datum design. In the experiments, the pressure side winglets offered an improvement in performance over the datum case in terms of peak power and hydrodynamic efficiency, though the power drop-off was more abrupt at low TSR with winglets. The suction surface winglets were inferior to the datum design in terms of both power coefficient and hydrodynamic efficiency.

Phase-locked PIV measurements were undertaken to investigate the loss sources in the rotor wake with different tip designs. It was found that the winglets had a significant impact on the amount of spanwise flow in the tip region. This spanwise flow leads to increased loss via secondary kinetic energy. The importance of spanwise flow in determining turbine performance highlights the need for fully 3D blade design codes.

The changes in axial secondary kinetic energy due to the winglets were found to be small. Because these changes occur at high radius, however, their impact on the blade root bending moment is likely to be large.

The discrepancy between the inviscid model predictions and the experimental results show that the performance of a winglet is determined by a combination of viscous and inviscid effects. Future work to investigate this includes a CFD study of the winglets tested for this work.

ACKNOWLEDGEMENT

The authors would like to thank the staff at Ifremer, Boulogne-sur-Mer for their help with the small-scale turbine measurements. The research leading to these results has received funding from the EPSRC and from the European Union Horizon 2020 Framework Programme (H2020) under grant agreement no 731084.

REFERENCES

[1] C. L. Sequeira, "Hydrodynamics of tidal stream turbines," Ph.D. dissertation, University of Cambridge, 2014.
[2] R. Whitcomb, "A design approach and selected wind-turbine results at high subsonic speed for wing-tip mounted winglets." NASA, Tech. Rep. TN D-8260, 1976.
[3] P. Gerontakos and T. Lee, "Effects of winglet dihedral on a tip vortex," *Journal of Aircraft*, vol. 43(1), pp. 117–124, 2006.
[4] D. Maniaci, "Wind turbine design using a free-wake vortex method with winglet application," Ph.D. dissertation, Pennsylvania State University, 2013.
[5] M. Maughmer, "The design of winglets for low-speed aircraft," Pennsylvania State University, Tech. Rep., 2005, invited talk given at the International Meeting of Light and Ultra Light Aircraft Design, Politecnico di Milano, Milan, Italy.
[6] J. Johansen and N. N. Sorensen, "Aerodynamic investigation of winglets on wind turbine blade using CFD," Riso National Laboratory, Tech. Rep. RISO-R-1543, 2006.
[7] T. Melin, "A vortex lattice matlab implementation for linear aerodynamic wing applications," Master's thesis, Royal Institute of Technology, Sweden, 2000.
[8] V. Bajpai, "The efficiency of tidal turbines," Master's thesis, University of Cambridge, 2018.
[9] C. L. Sequeira and R. Miller, "Loss mechanisms in tidal stream turbines," in *In Proceedings of the 10th European Wave and Tidal Energy Conference (EWTEC)*, 2013.
[10] M. Drela, "Power balance in aerodynamic flows," *AIAA Journal*, vol. 47, no. 7, 2009.